Interaction of Rarefaction Waves with Area Enlargements in Ducts

O. Igra* and J. J. Gottlieb†
Institute for Aerospace Studies, University of Toronto, Ontario, Canada

The interaction of a rarefaction wave with a gradual monotonic area enlargement of finite length in a duct is studied both analytically and numerically. An analytical quasisteady flow analysis is presented first, to obtain asymptotic solutions for the flow at late times, after all transient disturbances from the interaction process have subsided. Analytical results are presented and discussed for the boundary between the two possible predicted asymptotic wave patterns and the corresponding asymptotic strengths of the transmitted, reflected, and other waves, as a function of both the incident rarefaction-wave strength and area-enlargement ratio, for perfect diatomic gases and air. Finally, numerical results obtained using the random-choice method are presented and discussed for the complete nonstationary rarefaction-wave interaction with the area enlargement. These results show clearly how the transmitted, reflected, and other waves develop and evolve with time, until they eventually attain constant strengths, in agreement with the quasisteady flow predictions for the asymptotic wave patterns.

Introduction

MOVING shock and rarefaction waves that interact with area changes are a common feature of nonstationary gas flows encountered in engineering practice and research. For example, they occur in the piping system of reciprocating engines and pumps, in gas transportation pipelines, and in various shock tubes and blast-wave simulators that have an area change in the driver or channel (or at the diaphragm location). Although modern gasdynamic computer codes based on the method of characteristics, finite difference or finite element methods, and the random-choice method can now be used to solve such nonstationary internal flow problems,[1-3] mainly because of the advent of high-speed digital computers, it is important to study separately the simple interactions of shock and rarefaction waves with an area change in a duct. Fundamental knowledge gained from these studies is invaluable in interpreting the behavior of more complex flows.

The interaction of shock waves with area changes of finite length in ducts has been studied fairly thoroughly during the past three decades. Most of the early work incorporated a quasisteady flow analysis,[4-9] although some research employed a nonstationary flow analysis.[10,11] Only more recent work unites and exploits both types of analyses.[12] By contrast, no work of a similar nature is available for the case of a rarefaction wave interacting with an area change, although previous research[4-6,9,10] certainly contains relevant basic information.

The aim of this study is to use both the quasisteady and nonstationary flow analyses to obtain basic detailed results that apply, in general, to the case of a rarefaction wave interacting with an area enlargement. Attention is devoted to understanding the nature of the transient flow phenomena that eventually establish the quasisteady flow at late times, after all transient disturbances from the interaction process have subsided. This work is a sequel to recent studies involving the interaction of a rarefaction wave with an area reduction.[13,14] These studies are complementary, providing a clear picture of the nonstationary interaction process from early to late times for rarefaction waves passing through both gradual monotonic area reductions and enlargements.

Analytical and Numerical Analyses

Quasisteady Flow Analysis

A rarefaction wave moving in a quiescent gas toward an area enlargement in a duct is illustrated in Fig. 1. This wave produces a flow that moves in the opposite direction. Depending on the magnitudes of the area-enlargement ratio (S_d/S_u) and incident rarefaction-wave strength (pressure ratio p_2/p_1 across this wave), the rarefaction-wave interaction with the area enlargement will result in one of only two different possible postulated wave patterns shown schematically in Fig. 2. A transmitted rarefaction wave and a reflected shock wave appear in wave patterns A and B. Due to the existence of the shock wave, a contact surface or contact region also occurs in both patterns. An upstream-facing rarefaction wave appears only in pattern B, just downstream of the area

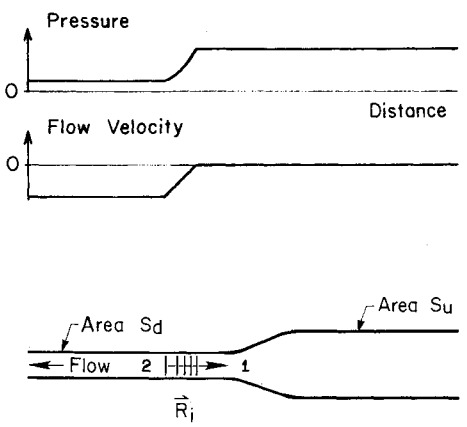

Fig. 1 Rarefaction wave moving toward an area enlargement in a duct.

Received August 3, 1983; revision received Aug. 17, 1984.

*Visiting Professor, from Ben-Gurion University of the Negev, Beer-Sheva, Israel.

†Associate Professor. Member AIAA.

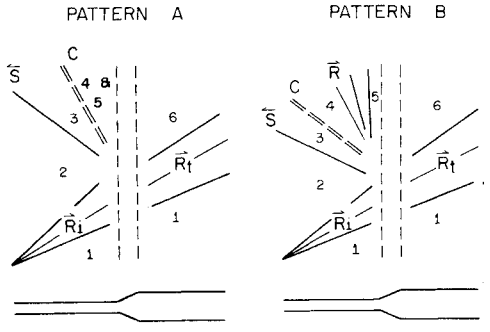

Fig. 2 Two different schematic quasisteady wave patterns for the interaction of a rarefaction wave with an area enlargement in a duct. (These are the only two possible wave patterns.)

change. Its head is stationary at the flow outlet of the area enlargement (sonic outflow), and the remainder of this wave is swept downstream.

The interaction of the incident rarefaction wave with the area enlargement is initially a nonstationary or an unsteady flow process. However, as local disturbances subside or disappear, through wave reflection and coalescing processes, the flow will eventually become quasisteady or steady. That is, the rarefaction and shock waves will eventually develop constant strengths and, at this stage, these waves and the contact region will separate fully developed regions of steady flow. The solution for the quasisteady flow properties for asymptotic wave patterns A and B can be obtained analytically, and the solution procedure is outlined herein.

For an inviscid flow of a perfect gas, the flow properties in regions 1 and 6 on either side of the transmitted rarefaction wave (see Fig. 2) are connected by an equation for a negatively sloped characteristic line crossing a simple rarefaction or expansion wave,[5,6,15]

$$\frac{2}{\gamma-1}\,a_6-u_6=\frac{2}{\gamma-1}\,a_1-u_1 \tag{1}$$

(with $u_1=0$), and the isentropic relations

$$p_6/p_1=[T_6/T_1]^{\gamma/(\gamma-1)}=[a_6/a_1]^{2\gamma/(\gamma-1)}=[\rho_6/\rho_1]^{\gamma} \tag{2}$$

The symbols p, T, a, ρ, u, and γ denote static pressure, temperature, sound speed, density, flow velocity, and specific-heat ratio, respectively. If the strength p_6/p_1 of the transmitted rarefaction wave is specified, for convenience instead of p_2/p_1 of the incident rarefaction wave, all of the flow properties in region 6 can be obtained directly from Eqs. (1) and (2), because the flow properties in region 1 are known initial conditions.

For a one-dimensional, isentropic, steady flow in the area enlargement, from region 6 to 5, the continuity and energy equations,[5,6,15]

$$\rho_5 u_5 S_d=\rho_6 u_6 S_u \tag{3}$$

$$h_5+u_5^2/2=h_6+u_6^2/2 \tag{4}$$

along with the sound-speed relation $a^2=\gamma RT=\gamma p/\rho$ and the enthalpy $h=C_pT$ or $h=\gamma RT/(\gamma-1)$, yield

$$p_5/p_6=[T_5/T_6]^{\gamma/(\gamma-1)}=[a_5/a_6]^{2\gamma/(\gamma-1)}=[\rho_5/\rho_6]^{\gamma}$$

$$=\left[\frac{M_6}{M_5}\,\frac{S_u}{S_d}\right]^{2\gamma/(\gamma+1)}=\left[\frac{2+(\gamma-1)M_6^2}{2+(\gamma-1)M_5^2}\right]^{\gamma/(\gamma-1)} \tag{5}$$

The symbols h, R, and M denote the specific enthalpy, gas constant, and flow Mach number (u/a), respectively. Because M_6 is dictated by previously determined information (u_6 and a_6) and the duct cross-sectional areas upstream (S_u) and downstream (S_d) of the area enlargement are specified, M_5 can be obtained from the last part of Eq. (5). Values of p_5, T_5, a_5, and ρ_5 then follow from the first part of Eq. (5), and u_5 is obtained from the product a_5M_5.

For the moment, consider only pattern A (Fig. 2), which does not have a downstream-swept rarefaction wave; pattern B will be considered later. The contact region in pattern A then separates regions 3 and 4 or 5. (Regions 4 and 5 are the same for pattern A.) Because the pressure and flow velocity remain unchanged across the contact region, the values of these flow properties in region 3 follow from $p_3=p_5$ and $u_3=u_5$. Other flow properties in region 3, such as the temperature and density, are not equal to those in region 5. They can be calculated as follows.

Region 2 lies between the tail of the incident rarefaction wave and the reflected shock wave. The flow properties in this region are related to those in region 3 by the Rankine-Hugoniot or shock relations,[5,6,15]

$$u_3=u_2-a_2(p_3/p_2-1)/[\gamma^2\beta(1+\alpha p_3/p_2)]^{1/2} \tag{6}$$

$$a_3=a_2[(p_3/p_2)(\alpha+p_3/p_2)]^{1/2}/[1+\alpha p_3/p_2]^{1/2} \tag{7}$$

in which $\alpha=(\gamma+1)/(\gamma-1)$ and $\beta=(\gamma-1)/2\gamma$. Furthermore, the flow properties in region 2 can be related to the known initial conditions in region 1, by using isentropic equations for the incident rarefaction wave. These equations are simply Eqs. (1) and (2) with subscript *6* changed to *2*.

Equations (6) and (7) and those mentioned for the incident rarefaction wave permit all of the flow properties in regions 2 and 3 to be determined, and thus the strength p_2/p_1 of the incident rarefaction wave, because values of p_3 and u_3 are already known from previously described calculations for pattern A. The relevant equations can be combined to yield

$$\left[\frac{p_2}{p_1}\right]^{\beta}=1+\gamma\beta\frac{u_3}{a_1}+\beta^{1/2}\left[\frac{p_2}{p_1}\right]^{\beta}$$

$$\times\left[\frac{p_3}{p_1}\,\frac{p_1}{p_2}-1\right]\left[1+\alpha\frac{p_3}{p_1}\,\frac{p_1}{p_2}\right]^{-1/2} \tag{8}$$

from which p_2/p_1 can be obtained readily by iteration. Values of T_2, a_2, ρ_2, and u_2 then follow from Eqs. (1) and (2) with the subscript *6* replaced by *2*. Finally, a_3 is obtained from Eq. (7), T_3 follows from a_3 by the sound-speed relation, and ρ_3 follows from p_3 and T_3 by means of the equation of state. This completes the development of the equations required for obtaining the flow properties and wave strengths for pattern A.

For the case of pattern B, the equations already introduced for pattern A simply need to be supplemented to account for the additional downstream-swept rarefaction wave (see pattern B in Fig. 2). The two supplemental equations that now connect regions 4 and 5 across this rarefaction wave are simply Eqs. (1) and (2) with subscripts *6* and *1* becoming *4* and *5*, respectively. Although these equations introduce additional variables, other variables disappear since the outflow from the area change for pattern B is sonic ($M_5=-1$), resulting in a similar but slightly modified calculation procedure with the same degree of difficulty as pattern A. Hence, further explanation is not required. This completes the development of the procedure required for pattern B.

The procedure for obtaining a complete set of flow properties for wave patterns A and B, for some specified area ratio, is now outlined. The solution for pattern A covers a

limited range of strengths of the incident and transmitted rarefaction waves. For the transmitted wave, the ratio p_6/p_1 takes on values from unity, for which there is no flow and all waves are Mach waves, to a minimum value of $\{p_6/p_1\}_{\min}$, when the transmitted wave is strongest. This minimum value corresponds to the condition when the flow is choked at the flow outlet of the area change ($M_5 = -1$). The value of $\{p_6/p_1\}_{\min}$ depends on the area-enlargement ratio, because it is equal to $[1-(\gamma-1)M_6/2]^{-1/\beta}$ from Eqs. (1) and (2), with M_6 given implicitly from $S_u/S_d = -M_6^{-1}\,[2/(\gamma+1)+M_6^2/\alpha]^{\alpha/2}$ from the latter part of Eq. (5) when $M_5 = -1$. Hence, a complete set of flow properties and the strength of the incident rarefaction wave can be obtained for pattern A by first specifying p_6/p_1 over the range from unity to $\{p_6/p_1\}_{\min}$ and then using the equations presented for pattern A, in the manner described.

The set of flow properties for pattern B, for a specified area ratio, can be calculated in the following manner. For this case the flow is always choked as it leaves the area change ($M_5 = -1$), and the strength of the transmitted rarefaction wave and the values of the flow properties in regions 5 and 6 are fixed. These limiting conditions with $M_5 = -1$ and $p_6/p_1 = \{p_6/p_1\}_{\min}$ are obtained from calculations for pattern A, by using Eqs. (1-5). For calculations of the flow properties in regions 2-4, it is most convenient to specify the strength p_4/p_5 of the downstream-swept rarefaction wave, instead of p_2/p_1 for the incident rarefaction wave. All of the flow properties in region 4 and then those in regions 2 and 3, including the strength of the incident rarefaction wave, can then be obtained from equations introduced earlier.

Nonstationary Flow Analysis

The continuity, momentum, and energy equations for one-dimensional, nonstationary, inviscid gas flows, written in conservation form, are[5,6,15]:

$$\frac{\partial}{\partial t}(\rho)+\frac{\partial}{\partial x}(\rho u) = -\frac{1}{S}\frac{\mathrm{d}S}{\mathrm{d}x}(\rho u) \tag{9}$$

$$\frac{\partial}{\partial t}(\rho u)+\frac{\partial}{\partial x}(\rho u^2+p) = -\frac{1}{S}\frac{\mathrm{d}S}{\mathrm{d}x}(\rho u^2) \tag{10}$$

$$\frac{\partial}{\partial t}(e)+\frac{\partial}{\partial x}(ue+up) = -\frac{1}{S}\frac{\mathrm{d}S}{\mathrm{d}x}(ue+up) \tag{11}$$

where x, t, S, and e denote distance, time, duct cross-sectional area, and total energy per unit volume, respectively. The total energy is the sum of the internal energy $\rho C_v T$ and kinetic energy $\rho u^2/2$, which is often expressed as $p/(\gamma-1)+\rho u^2/2$ for a perfect gas. This set of equations is completed by the thermal equation of state for a perfect gas, i.e., $p=\rho RT$.

For computations for the problem of a rarefaction wave interacting with an area enlargement in a duct, the specific variation of area $S(x)$ is required. In this study the area change between two constant-area ducts of upstream area S_u and downstream area S_d is specified by

$$S(x) = S_d \exp[\ell n (S_u/S_d)^{1/2}(1-\cos\{\pi x/\delta\})] \tag{12}$$

where $x=0$ at the small end (S_d) and $x=\delta$ at the large end (S_u). This particular area change of finite length δ has a monotonic transition and can be used for both an enlargement and a reduction. It was chosen because

$$\frac{1}{S}\frac{\mathrm{d}S}{\mathrm{d}x} = \frac{\pi}{2\delta}\ell n\frac{S_u}{S_d}\sin\frac{\pi x}{\delta} \tag{13}$$

is a symmetric, sinusoidal transition, which is advantageous over asymmetrical variations in reducing numerical noise in the computed flowfield properties.

Equations (8-12) are solved numerically in the present study using the random-choice method (RCM) invented by Glimm[17] and first applied by Chorin,[18] which is well suited for solving such problems. Shock waves and contact surfaces are well defined with sharp fronts in this method, unlike finite difference methods where they are normally smeared out over many mesh zones, due to the effects of explicit artificial and implicit numerical viscosities. The operator-splitting technique introduced to the RCM by Sod,[19] in order that one-dimensional flow problems with area changes could be solved, is also employed in this study. Note that the RCM is a first-order, explicit, numerical scheme that repeatedly solves a Riemann or shock-tube problem between two grid points, and details of this method can be found elsewhere.[3,17-19]

Results and Discussion

Quasisteady Flow

For the interaction of a rarefaction wave with an area enlargement in a duct (Fig. 1), two different wave patterns shown schematically in Fig. 2 were postulated. Based on the quasisteady flow analysis presented earlier, the domains and boundary for these two patterns can be calculated as a function of the incident rarefaction-wave strength p_2/p_1 and the duct area ratio S_d/S_u. The boundary corresponds to the conditions when the flow is choked ($M_5 = -1$) and the downstream-swept rarefaction wave is a Mach wave ($p_4 = p_5$). Results obtained for perfect diatomic gases and air with $\gamma = 7/5$ are given in Fig. 3. Additional results for monatomic gases with $\gamma = 5/3$ and a polyatomic gas with $\gamma = 11/10$ are also shown to illustrate the effects of the specific-heat ratio. Patterns A and B are the only two wave patterns that can exist.

The strength p_6/p_1 of the transmitted rarefaction wave is shown in Fig. 4, in terms of the incident rarefaction-wave strength p_2/p_1 and area-enlargement ratio S_d/S_u, for perfect diatomic gases and air with $\gamma = 7/5$. The domains corresponding to patterns A and B are indicated and separated by a dashed line. As p_2/p_1 decreases from unity to zero, for a specific value of S_d/S_u, p_6/p_1 first decreases from unity to $\{p_6/p_1\}_{\min}$ in region A and then remains constant at this latter value throughout region B. Because the flow at the outlet of the area change is choked for region B, the strength of the

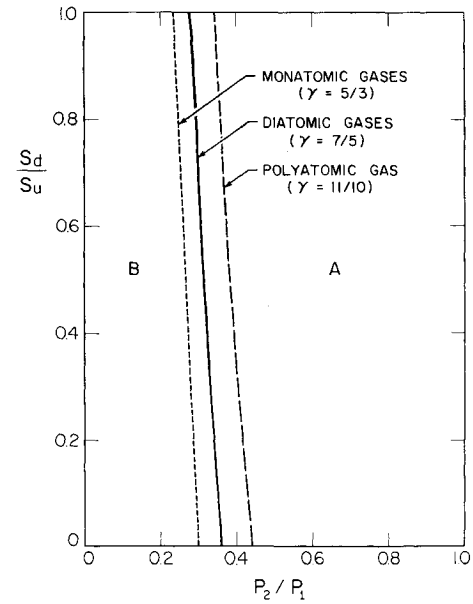

Fig. 3 Domains and boundary for wave patterns A and B for the interaction of a rarefaction wave of incident pressure ratio p_2/p_1, with an area enlargement of ratio S_d/S_u for perfect gases.

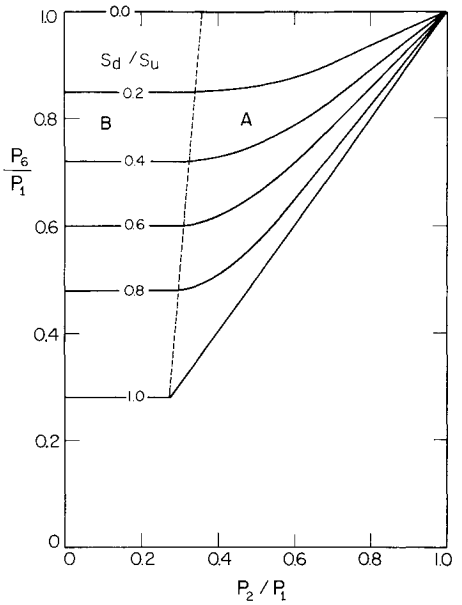

Fig. 4 Strength p_6/p_1 of the transmitted rarefaction wave, shown as a function of the incident rarefaction-wave strength p_2/p_1 and area-enlargement ratio S_d/S_u, for perfect diatomic gases and air with $\gamma = 7/5$.

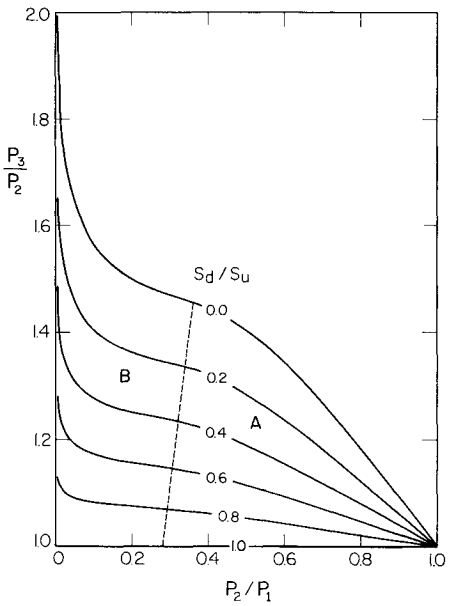

Fig. 5 Strength p_3/p_2 of the reflected shock wave, shown as a function of the incident rarefaction-wave strength p_2/p_1 and area-enlargement ratio S_d/S_u, for perfect diatomic gases and air with $\gamma = 7/5$.

transmitted wave remains constant. The transmitted rarefaction wave is weaker than the incident rarefaction wave for a fixed area ratio because p_6/p_1 is larger than p_2/p_1. For a fixed strength of the incident wave, an increase in the area-enlargement ratio results in a stronger transmitted wave. The transmitted wave is merely a Mach wave when the area ratio S_d/S_u is zero (i.e., S_u is infinitely larger than S_d), and it is strongest when $S_d/S_u = 1$ (no change in duct area). For this case with pattern A, the incident rarefaction wave merely becomes the transmitted rarefaction wave, resulting in p_6/p_1 being equal to p_2/p_1 (as expected for a constant-area duct). For the case of pattern B, the first part of the incident wave from its head (zero flow) to the point within the wave where the flow is sonic becomes the transmitted wave, and the remainder from the sonic point to the tail (where the flow is supersonic) becomes the upstream-facing but downstream-swept rarefaction wave.

The strength p_3/p_2 of the reflected shock wave is shown in Fig. 5, also as a function of both the incident rarefaction-wave strength and area-enlargement ratio. For no change in cross-sectional area ($S_d/S_u = 1$) the reflected shock wave is merely a Mach wave or nonexistent ($p_3/p_2 = 1$). As the change in area becomes larger (S_d/S_u decreases) and the incident rarefaction wave becomes stronger (p_2/p_1 decreases), the strength p_3/p_2 of the reflected shock wave increases, as could be expected. It can be seen that the reflected shock wave is generally quite weak (i.e., p_3/p_2 is less than 1.5), unless the incident rarefaction wave is almost a complete expansion wave with a strength p_2/p_1 very close or equal to zero. Results of the quasisteady analysis also showed that changes in density, temperature, and entropy across the contact region were negligibly small. This means that a reflected compression wave instead of a reflected shock wave could have been used in the quasisteady flow analysis, provided that values of p_2/p_1 were not too close to zero, and the calculated flow properties would have been virtually the same. For practical purposes, it is inconsequential as to whether the reflected wave is taken to be a shock or compression wave in the quasisteady flow analysis (for $p_2/p_1 > 0.01$).

Finally, the strength p_4/p_5 of the downstream-swept rarefaction wave of pattern B is shown in Fig. 6, also as a function of p_2/p_1 and S_d/S_u. For a fixed area ratio, p_4/p_5 decreases almost linearly with decreasing values of p_2/p_1, from unity (at

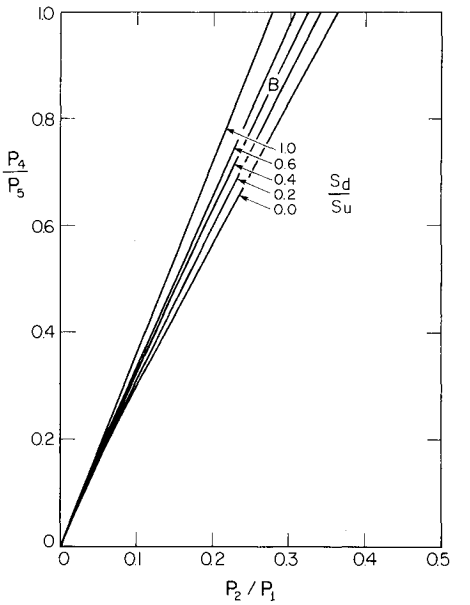

Fig. 6 Strength p_4/p_5 of the downstream-swept rarefaction wave of pattern B, shown as a function of the incident rarefaction-wave strength p_2/p_1 and area-enlargement ratio S_d/S_u, for perfect diatomic gases and air with $\gamma = 7/5$.

the boundary between patterns A and B) to zero when $p_2/p_1 = 0$. For a fixed incident rarefaction-wave strength, the downstream-swept rarefaction wave is stronger when the area change is more severe. However, the downstream-swept rarefaction wave is always weaker than the incident rarefaction wave. This should be expected because the origin of this downstream-swept rarefaction wave is the latter part of the incident rarefaction wave. Although this part of the wave passes through the reflected shock wave and contact region, being somewhat altered in the process, it cannot move forward against the supersonic flow (in region 5) and into the area enlargement.

Nonstationary Flow

Numerical results obtained by using the RCM for solving the interaction of a rarefaction wave with an area enlargement are now presented graphically and discussed, to illustrate how the transmitted, reflected, and other waves form, evolve with time, and eventually attain constant strengths as they become quasisteady, in agreement with the quasisteady flow predictions for the asymptotic wave patterns. Computations were made for many different combinations of values of the incident rarefaction-wave strength and area-enlargement ratio; however, only a few typical results can be presented here. Additional numerical results for perfect diatomic gases ($\gamma = 7/5$), as well as additional quasisteady flow solutions for perfect monatomic gases ($\gamma = 5/3$), can be found in a UTIAS report.[16]

Numerical results obtained with the RCM are given in Figs. 7 and 8 in the form of separate sets of spatial distributions for nondimensional pressure p/p_1 and flow velocity u/a_1. Each successive distribution is displaced upward from the previous one, so that the effect of a time-distance diagram is produced. The nondimensional time interval between successive distributions is given by $\Delta\tau = a_1 \Delta t/\delta$, and the nondimensional value of $\Delta\tau$ for each case is given in the caption of each figure. The location of the area enlargement of length δ is indicated by the two vertical dashed lines. The incident rarefaction wave is initially specified in the bottom distribution of each set, just to the left of the area enlargement. In each case it is distributed over a distance of nine-tenths of the length of the area change or $9\delta/10$. The initial flow velocity is specified to change linearly over this spatial interval, and the other flow properties can be derived from this variation and the specification of the incident rarefaction-wave strength p_2/p_1. Such a specification of the spatial properties of the incident rarefaction wave means that it was originally a centered rarefaction wave at some earlier distance and time. The flowfield is computed with 720 grid zones, of which 20 zones are allocated to the area enlargement and 18 are allocated to the incident rarefaction-wave profile.

Graphical results for density, temperature, and entropy are not presented, since they do not provide significant additional information, for the following reasons. In each example the flow is essentially isentropic and changes in the flow properties across the contact region are negligibly small, because the reflected shock wave is relatively weak. Hence, the entropy is essentially constant throughout the flowfield, and sets of spatial distributions for density and temperature are very

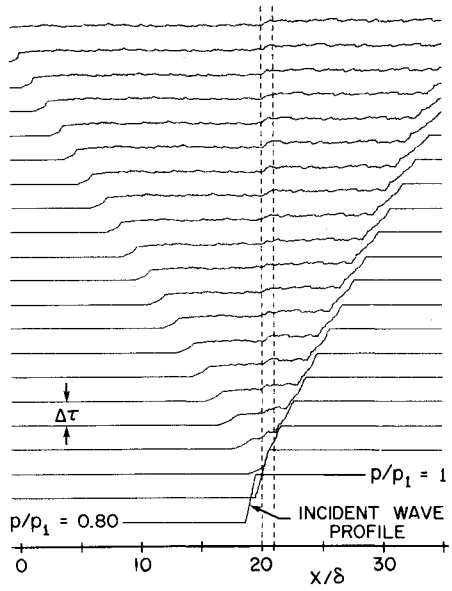

a) Pressure p/p_1

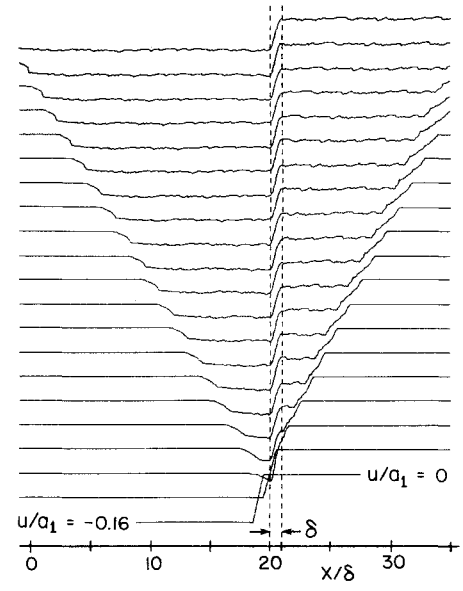

b) Flow velocity u/a_1

Fig. 7 Spatial distributions of pressure (a) and flow velocity (b) for the interaction of a rarefaction wave with an area enlargement ($p_2/p_1 = 0.80$, $S_d/S_u = 0.50$, $\Delta\tau = 1.04$, pattern A). Note that δ is the area enlargement length and $\Delta\tau = a_1 \Delta t/\delta$ the nondimensional time between successive spatial distributions.

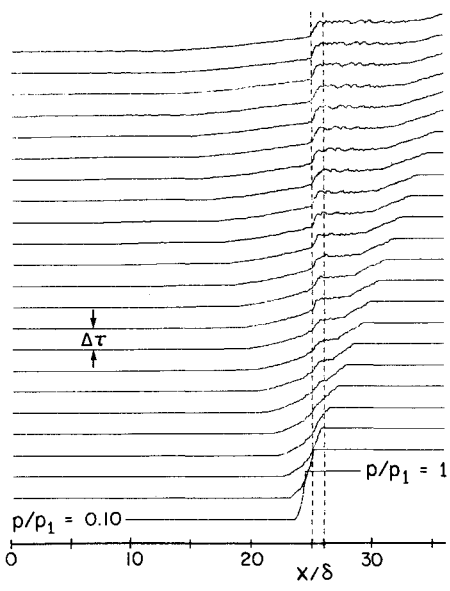

a) Pressure p/p_1

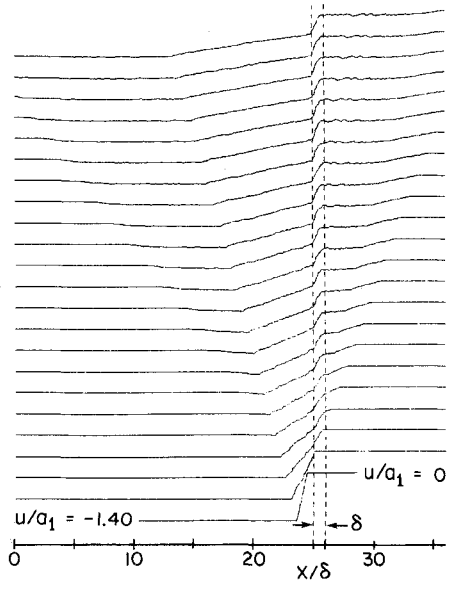

b) Flow velocity u/a_1

Fig. 8 Spatial distributions of pressure (a) and flow velocity (b) for the interaction of a rarefaction wave with an area enlargement ($p_2/p_1 = 0.10$, $S_d/S_u = 0.50$, $\Delta\tau = 0.67$, pattern B).

similar to those for the pressure. In fact, the density and temperature can be obtained from the pressure, for all practical purposes, by using the usual isentropic equations like those given by Eq. (2).

The first set of numerical results for the pressure and flow velocity appears in Fig. 7, for the case of $p_2/p_1 = 0.80$ and $S_d/S_u = 0.50$, corresponding to a point near the center of the domain of pattern A (Fig. 3). The incident rarefaction wave is shown clearly in the bottom distribution, just prior to its impingement on the area enlargement. Its subsequent interaction with the area change can be observed in the following distributions, where the formation and evolution of the transmitted rarefaction wave and reflected shock wave can be seen clearly, as well as the eventual development of steady subsonic flow in and on both sides of the area change. It is evident that the reflected wave is initially a compression wave, whose front becomes steeper as it propagates away from the area change, and it is obvious that a steep-fronted shock wave will eventually be formed (not shown). Note that the steady flow in the area change at later times is an expected subsonic nozzle flow, as the gas flows through the convergence in area (from right to left) the pressure decreases and the flow velocity increases (becomes more negative).

Other numerical results corresponding to points in pattern A are similar to those just presented; they are not given here for brevity but can be found elsewhere.[16] The main difference is that the reflected wave becomes weaker and takes longer to form into a steep-fronted shock wave as the area enlargement becomes less severe ($S_d/S_u \to 1$), and conversely.

The second set of numerical results is presented in Fig. 8, for the case of $p_2/p_1 = 0.10$ and $S_d/S_u = 0.50$, corresponding to a point near the center of the domain of pattern B. The incident rarefaction is again shown in the bottom distribution. Its subsequent interaction with the area change can be observed in the following distributions, where the formation and evolution of the transmitted and downstream-swept rarefaction waves can be seen clearly. Both of these waves are spreading out at later times, and a quasisteady flow region of increasing lateral extent develops between the transmitted wave and the area change. The reflected compression wave is just noticeable, mainly because the other waves are much stronger and the pressure scale has been much compressed. Any steepening of this compression wave in the computed flowfield is barely visible. For this example, the strong incident rarefaction wave produces a sufficiently low pressure downstream of the area change such that the flow is first accelerated to sonic or choked conditions at the flow outlet of the area change. This flow is then accelerated further to supersonic speeds through the downstream-swept rarefaction wave.

Other numerical results corresponding to points in pattern B are similar; they are not given here for brevity but can be found elsewhere.[16] The main differences are that the reflected wave becomes stronger and can be seen to steepen into a shock wave as the area change becomes more severe ($S_d/S_u \to 0$), and the lateral spreading of the fans of the transmitted and downstream-swept rarefaction waves are larger or smaller, depending on their strength.

It is apparent from the numerical results given in Figs. 7 and 8 that the wave pattern that emerges at late times is pattern A for Fig. 7 and pattern B for Fig. 8, in agreement with the initial values of p_2/p_1 and S_d/S_u selected in each quasisteady domain of patterns A or B. This was also true for all other numerical results for values of p_2/p_1 and S_d/S_u that correspond to points in the domains of quasisteady wave patterns A and B, even when points were taken close to the boundary between patterns A and B.

Although it is not readily obvious from the numerical results given in Figs. 7 and 8 (and others shown elsewhere[16]), pattern A emerges fairly quickly in the numerical results and pattern B takes somewhat longer. Computed flow properties in various quasisteady flow regions and strengths of rarefaction and shock waves converge fairly rapidly to those

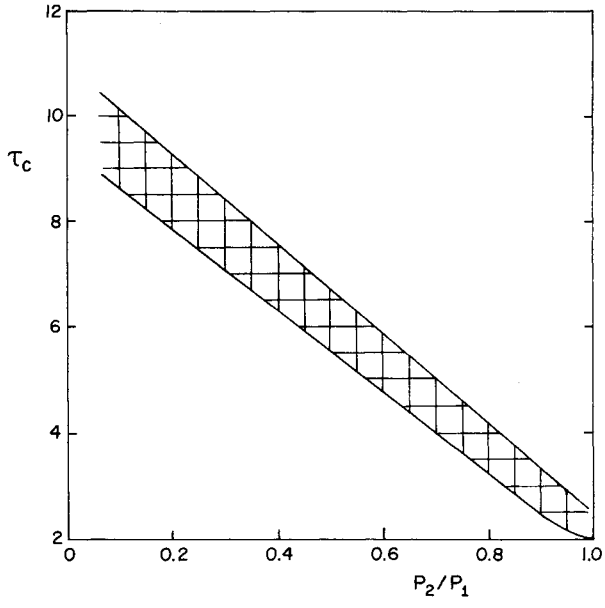

Fig. 9 Characteristic time $\tau_c = a_1 t_c/\delta$ vs incident rarefaction-wave strength p_2/p_1 for the initially nonstationary flow to eventually become almost quasisteady.

predicted by the quasisteady flow analysis for pattern A and somewhat longer for pattern B, for the following reason. An initial part of the incident rarefaction wave first establishes pattern A which is then altered or extended to pattern B by the latter part of the incident rarefaction wave. This alteration takes time to occur, especially if the incident rarefaction wave is strong.

The time for the nonstationary flow to become quasisteady and establish pattern A or B has been discussed only qualitatively. In order to obtain quantitative results, a definition of a characteristic time is needed. Let the characteristic time t_c be defined as the time interval measured from when the incident rarefaction wave first encounters the area enlargement until the nonstationary flow properties in quasisteady flow regions between distinct waves are within 5% of the quasisteady flow predictions. Based on this definition, the nondimensional characteristic time $\tau_c = a_1 t_c/\delta$ obtained from many numerical results are shown vs the incident rarefaction-wave strength in Fig. 9. The characteristic times, shown as a band, increase for stronger incident rarefaction waves or decreasing values of p_2/p_1. This should be expected since a stronger rarefaction wave has a wider fan of characteristics that would take longer to complete its interaction with the area enlargement.

The characteristic times are presented in the form of a band for the following reasons. First, the choice of a characteristic time from numerically predicted results for the nonstationary flow properties to come within 5% of the quasisteady flow predictions is somewhat arbitrary, because the numerical results contain numerical noise or random fluctuations that are characteristic of the RCM. Hence, precise values could not be obtained in the present work. Second, the characteristic times were found to be weakly dependent on the area-enlargement ratio, which could not be determined with precision from the numerical results. However, the general trend was that characteristic times were slightly longer for more severe area enlargements, for a given value of p_2/p_1.

Concluding Remarks

The interaction of rarefaction waves with gradual, monotonic area enlargements in ducts has been studied by using two complementary analyses. The quasisteady flow

analysis that describes the flow behavior at late times was instrumental in establishing the two asymptotic wave patterns, including the asymptotic values of the quasisteady flow properties and the asymptotic strengths of the transmitted, reflected, and other waves, as a function of both the incident rarefaction-wave strength and area-enlargement ratio. The nonstationary flow analysis was necessary for determining the transient flow behavior from early to late times and showing how the quasisteady flow was eventually established. The random-choice method was found to be excellent for solving this nonstationary flow problem.

The nonstationary flow analysis showed that the asymptotic wave patterns were established fairly rapidly for pattern A and somewhat longer for pattern B (see Fig. 9). Consequently, the quasisteady flow analysis can be used to give a good estimate of the flow properties and strengths of the transmitted, reflected, and other waves at relatively early times, which would have practical implications. However, when a detailed study of the transient wave behavior is needed, the nonstationary flow analysis is required to obtain more accurate flowfield predictions.

The flow was assumed to be one-dimensional for both the quasisteady and nonstationary flow analyses. This assumption is reasonable for flowfield calculation of the interaction of a rarefaction wave with an area enlargement for the following reason. The flow in the area change is a typical subsonic nozzle flow in which flow separation is suppressed by a favorable pressure gradient. Although viscous effects would become important for severe area changes, these effects have been ignored.

Acknowledgments

The authors would like to thank Dr. T. Saito for his help in obtaining the numerical results with the RCM and Mr. P. M. Ostaff for his assistance with the quasisteady flow computations. The financial support received mainly from the Defence Research Establishment Suffield and partly from the Natural Sciences and Engineering Research Council, both of Canada, is much appreciated.

References

[1]Jones, A. D. and Brown, G. L., "Determination of Two-Stroke Engine Exhaust Noise by the Method of Characteristics," *Journal of Sound and Vibration,* Vol. 82, June 1982, pp. 305-327.

[2]Beam, R. M. and Warming, R. F., "An Implicit Factored Scheme for the Compressible Navier-Stokes Equations," *AIAA Journal,* Vol. 16, April 1978, pp. 393-402.

[3]Saito, T. and Glass, I. I., "Applications of Random-Choice Method to Problems in Shock and Detonation-Dynamics," Institute for Aerospace Studies, University of Toronto, Canada, UTIAS Rept. 240, Oct. 1979.

[4]Kahane, A., Warren, W. R., Griffith, W.C., and Marino, A. A., "A Theoretical and Experimental Study of Finite Wave Interactions with Channels of Varying Area," *Journal of the Aeronautical Sciences,* Vol. 21, Aug. 1954, pp. 505-525.

[5]Rudinger, G., *Wave Diagrams for Nonsteady Flow in Ducts,* D. van Nostrand Co., New York, 1955.

[6]Rudinger, G., *Nonsteady Duct Flow: Wave-Diagram Analysis,* Dover Publications, New York, 1969.

[7]Oppenheim, A. K., Urtiew, P. A., and Stern, R. A., "Peculiarity of Shock Impingement on Area Convergence," *The Physics of Fluids,* Vol. 2, July-Aug. 1959, pp. 427-431.

[8]Chester, W., "The Propagation of Shock Waves Along Ducts of Varying Cross Section," *Advances in Applied Mechanics,* Vol. 6, Academic Press, New York, 1960, pp. 119-152.

[9]Oppenheim, A. K., Urtiew, P. A., and Laderman, A. J., "Vector Polar Method for the Evaluation of Wave Interaction Processes," *Archiwum Budowy Maszyn* (The Archive of Mechanical Engineering), Vol. XI, No. 3, 1964, pp. 441-495.

[10]Bannister, F. K. and Mucklow, G. F., "Wave Action Following Sudden Release of Compressed Gas from a Cylinder," *Proceedings of Industrial and Mechanical Engineering,* Vol. 159, 1948, pp. 269-300.

[11]Rudinger, G., "Passage of Shock Waves through Ducts of Variable Cross Section," *The Physics of Fluids,* Vol. 3, May-June 1960, pp. 449-455.

[12]Greatrix, D. R. and Gottlieb, J. J., "An Analytical and Numerical Study of a Shock Wave Interaction with an Area Change," Institute for Aerospace Studies, University of Toronto, Canada, UTIAS Rept. 268, Nov. 1982.

[13]Gottlieb, J. J. and Saito, T., "An Analytical and Numerical Study of the Interaction of Rarefaction Waves with Area Changes in Ducts—Part 1: Area Reductions," Institute for Aerospace Studies, University of Toronto, Canada, UTIAS Rept. 272, Nov. 1983.

[14]Gottlieb, J. J. and Igra, O., "Interaction of Rarefaction Waves with Area Reductions in Ducts," *Journal of Fluid Mechanics,* Vol. 137, Dec. 1983, pp. 285-305.

[15]Owczarek, J. A., *Fundamentals of Gasdynamics,* International Textbook Co., Scranton, Pa., 1964.

[16]Igra, O., Gottlieb, J. J., and Saito, T., "An Analytical and Numerical Study of the Interaction of Rarefaction Waves with Area Changes in Ducts—Part 2: Area Enlargement," Institute for Aerospace Studies, University of Toronto, Canada, UTIAS Rept. 273, Dec. 1984.

[17]Glimm, J., "Solution in the Large for Nonlinear Hyperbolic Systems of Equations," *Communications on Pure and Applied Mathematics,* Vol. 18, Nov. 1965, pp. 697-715.

[18]Chorin, A. J., "Random Choice Solution of Hyperbolic Systems," *Journal of Computational Physics,* Vol. 22, Dec. 1976, pp. 517-533.

[19]Sod, G. A., "A Numerical Study of a Converging Cylindrical Shock," *Journal of Fluid Mechanics,* Vol. 83, Pt. 4, pp. 785-794.